

Band-filling effects on electron-phonon properties of normal and superconducting statesE. Cappelluti,^{1,2} S. Ciuchi,³ C. Grimaldi,⁴ and L. Pietronero^{2,5}¹*“Enrico Fermi” Center, v. Panisperna, 00184 Roma, Italy*²*Dipart. di Fisica, Università di Roma “La Sapienza,” Piazzale A. Moro, 2, 00185 Roma, and INFM UdR Roma1, Italy*³*Dipart. di Fisica, Università dell’Aquila, v. Vetoio, 67010 Coppito-L’Aquila, and INFM, UdR L’Aquila, Italy*⁴*Institut de Production et Robotique, LPM, École Polytechnique Fédérale de Lausanne, CH-1015 Lausanne, Switzerland*⁵*Istituto di Acustica “O.M. Corbino,” CNR, Area di Ricerca Tor Vergata, Roma, Italy*

(Received 19 February 2003; revised manuscript received 24 June 2003; published 7 November 2003)

We address the effect of band filling on the effective electron mass m^* and the superconducting critical temperature T_c in an electron-phonon system. We compare the vertex corrected theory with the noncrossing approximation of the Holstein model within a local approximation. We identify two regions of the electron density where m^* and T_c are enhanced or decreased by the inclusion of the vertex diagrams. We show that the crossover between the enhancement at low density and the decrease towards half filling is almost independent of the microscopic electron-phonon parameters. These different behaviors are explained in terms of the net sign of the vertex diagrams which is positive at low densities and negative close to half filling. Predictions of the present theory for doped MgB_2 , which is argued to be in the low density regime, are discussed.

DOI: 10.1103/PhysRevB.68.174509

PACS number(s): 63.20.Kr, 74.20.-z, 71.38.Cn

I. INTRODUCTION

Recently, the discovery of superconductivity at $T_c \simeq 39$ K in magnesium diboride MgB_2 ,¹ has stimulated strong interest in the role of band filling in phonon-driven superconductivity when the charge carriers stem from low electron or hole density in the conduction band. Classical examples of low density superconductors are doped semiconductors such as GeTe which display critical temperatures T_c of the order of 1 K or less. Such small T_c values are understood as basically due to low values of the density of states at the Fermi level N_0 which goes to zero as $N_0 \propto \sqrt{E_F}$, where E_F is the Fermi energy. In this case, the electron-phonon coupling, which scales with the density of states $\lambda = g^2 N_0$, where g is the electron-phonon matrix element, also vanishes as $\lambda \propto \sqrt{E_F}$. This situation changes drastically for systems having a marked two-dimensional character of the conduction band at the Fermi level. In fact, an ideal two-dimensional system has a finite value of N_0 even when $E_F \rightarrow 0$, leading in principle to a sizeable λ also for very low charge carrier concentrations.

Magnesium diboride belongs, in principle, to such a class of materials. In fact, the peculiarity of MgB_2 resides in its electronic band structure which is built up by three-dimensional π bands and quasi-two-dimensional σ bands.^{2,3} Both sets of bands have large bandwidths of the order of 5–10 eV, however, the Fermi energy cuts the σ band quite near the band edge leading to E_F of only 0.4–0.6 eV. Since the Fermi level crosses the σ bands around the Γ point, the low-energy physics of the σ bands is essentially captured by a simple parabolic band structure corrected by a small interplane hopping element.³ The electron-phonon coupling has been estimated by several groups and the common agreement is that the σ bands are strongly coupled to lattice vibrations of E_{2g} symmetry and frequency ω_{ph} of order 70 meV, while the π bands have a somewhat lower interaction.^{4–6} Hence, the main features of MgB_2 can be de-

scribed by a quasi-two-dimensional parabolic band with low density of holes interacting with the lattice vibrations.

After the discovery of $T_c = 39$ K in MgB_2 , the idea of varying the hole density of the σ bands to possibly enhance T_c has been the object of several works, both theoretical and experimental. A possible route is to provide additional charge, electrons, or holes, to the system by chemical substitution of Mg or B atoms, although the rigid band scheme is somehow questionable. For instance, by substituting Mg with Al it is possible to further decrease the Fermi energy of the pure MgB_2 (Refs. 7,8) and consequently to explore the nonadiabatic regime. It is interesting to see that by increasing the Al content the critical temperature decreases^{7,8} but not at the rate expected by first principles calculations carried on with Eliashberg scheme.⁹

An alternative way to chemical substitution is to search for related compounds with similar electronic properties. For example, insulating LiBC compounds have been theoretically predicted to display high values of the superconducting critical temperature T_c for low hole dopings corresponding to $E_F < 0.5$ eV.¹⁰

Such small values of E_F together with sizeable electron-phonon couplings define a highly nontrivial situation for which the classical Migdal-Eliashberg (ME) theory becomes questionable. A major inadequacy of the classical theory is the breakdown of the adiabatic hypothesis occurring when the Fermi energy becomes of the same order or smaller than the characteristic phonon frequency scale $E_F \lesssim \omega_{\text{ph}}$ (Ref. 11) or when λ becomes strong enough to give rise to polaronic effects.¹² So far this issue has often been associated with narrow band systems, such as fullerenes,¹³ cuprates,¹⁴ and manganites,¹⁵ where the Fermi energy is constrained by the small electronic bandwidth.

As discussed above, however, the nonadiabatic problem can also be relevant in large band materials with low carrier density provided a nonvanishing electron-phonon coupling λ . The nonadiabatic degree ω_{ph}/E_F can thus be tuned by varying the charge carrier density or alternatively the chemi-

cal potential through the electronic band up to the top (or the bottom) of the electronic states.

The aim of the present paper is to investigate the onset of nonadiabatic effects in large band systems as a function of the charge density in detail and their implications on the superconducting and normal state properties. We find two regions of the electronic filling in which nonadiabatic contributions behave in qualitatively different manners: at sufficiently low density they enhance the electron-phonon effects in normal and superconducting state properties, while close to half-filling nonadiabatic effects basically lead to a weakening.

II. NONADIABATIC THEORY: NONCROSSING AND VERTEX CORRECTION APPROXIMATIONS

In this section we present a brief summary of the theory of nonadiabatic superconductivity in term of the Green's function formalism,¹⁶ where the nonadiabatic effects will be introduced at different stages of complexity. An explicit analytical derivation of the superconducting equations will be provided within the local approximation.

Let us consider a single band electron system interacting with phonons. In the normal state, the electron propagator is

$$G(k)^{-1} = i\omega_n - \epsilon_{\mathbf{k}} + \epsilon_0 - \Sigma(k), \quad (1)$$

where $\omega_n = (2n+1)\pi T$ is the fermionic Matsubara frequency, T is the temperature, $\epsilon_{\mathbf{k}}$ is the electron dispersion, ϵ_0 the chemical potential, and $\Sigma(k)$ is the electronic self-energy. In Eq. (1), the index k stands for the four-momentum (\mathbf{k}, ω_n) . In the following, we assume that the Coulomb contribution to the normal state self-energy has already been absorbed in the electron dispersion and the chemical potential. However, for the moment, we do not need to specify the form of $\epsilon_{\mathbf{k}}$. The electron self-energy $\Sigma(k)$ is determined by the electron-phonon interaction

$$\Sigma(k) = \sum_{k'} V_N(k, k') G(k'), \quad (2)$$

where $\Sigma_{k'} = -(T/N)\Sigma_m \Sigma_{\mathbf{k}'}$. Up to the first order of the irreducible electron-phonon interaction, the kernel of the self-energy $V_N(k, k')$ is given by^{17,18}

$$\begin{aligned} V_N(k, k') &= V(k, k') + V(k, k') \\ &\times \sum_{k''} V(k, k'') G(k'') G(k'' - k + k'). \end{aligned} \quad (3)$$

In the above expression, the lowest order electron-phonon interaction $V(k, k')$ is given by $V(k, k') = g(\mathbf{k}, \mathbf{k}')^2 D(k - k')$, where $g(\mathbf{k}, \mathbf{k}')$ is the electron-phonon matrix element and $D(k - k')$ is the phonon propagator. In the following, we assume a phenomenological model for $D(k - k')$, in the same spirit of Migdal-Eliashberg theory in which the phononic degrees of freedom are taken from experiments while the electron Green's function is calculated self-consistently. Hence, we shall not consider the effects of the

phonon self-energy. These are, however, negligible at sufficiently low electron densities which is the region of main interest to us.

If the second term in Eq. (3) is neglected, the so-called noncrossing approximation (NCA) is recovered which, in the limit of infinite bandwidth, is equivalent to the Migdal-Eliashberg approximation.^{11,19} In the following we shall use the terminology "noncrossing approximation" in order to make clear the diagrammatic meaning of such approximation in comparison with higher order theories. When the full expression of Eq. (3) is considered, the system is described within the vertex-corrected approximation (VCA), equivalent to the theory of nonadiabatic electron-phonon interaction discussed in Refs. 16–18. For later convenience, and to maintain a closer connection with the notation used in Ref. 16–18, we define the vertex function

$$P(k, k') = \sum_{k''} V(k, k'') G(k'') G(k'' - k + k'), \quad (4)$$

so that Eq. (3) is simply

$$V_N(k, k') = V(k, k') [1 + P(k, k')]. \quad (5)$$

The extensions of NCA and VCA to describe the superconducting transition are readily obtained by either introducing the Nambu formalism or by computing the pairing susceptibility. We adopt the latter formalism here so that the temperature T_c at which the pairing susceptibility diverges is given by the solution of the following secular equation:

$$\phi(k) = \sum_{k'} V_{\Delta}(k, k') G(k') G(-k') \phi(k'), \quad (6)$$

where $\phi(k)$ is the off-diagonal self-energy and the kernel V_{Δ} is

$$\begin{aligned} V_{\Delta}(k, k') &= V(k, k') + V(k, k') \\ &\times \sum_{k''} V(k, k'') G(k'') G(k'' - k + k') + V(k, k') \\ &\times \sum_{k''} V(k'', k) G(-k'') G(-k'' + k - k') \\ &+ \sum_{k''} V(k, k'') V(k'', k') G(k'') G(k'' - k - k'). \end{aligned} \quad (7)$$

The NCA equations are obtained by neglecting all the nonadiabatic corrections so that $V_{\Delta}(k, k')$ is simply $V(k, k')$. In this limiting case the electron-phonon interaction enters in the same way in the interaction kernels of both the self-energy and the superconducting pairing: $V_{\Delta}(k, k') = V_N(k, k') = V(k, k')$. This is, however, not true in the VCA framework where, in principle, $V_{\Delta}(k, k') \neq V_N(k, k')$. In particular the nonadiabatic terms add considerable structure to the pairing kernel but symmetry considerations permit us to simplify the structure of $V_{\Delta}(k, k')$. In fact, if the system has inversion symmetry $V(k, k') = V(-k, -k')$ and $G(-k)$

$=G(k)^*$, where $G(k)^*$ is the complex conjugate of $G(k)$. By using these relations it is easy to see that the third term on the right-hand side of Eq. (7) is the complex conjugate of the second term. Their sum is therefore twice the real part of, for example, the second term. Consider now the last term of Eq. (7). If we replace the summed index k'' with $-k''+k-k'$ then the resulting expression is equal to the complex conjugate of the original term. Then the last term of the gap equation is also real. These considerations permit us to rewrite Eq. (7) in the more condensed form

$$V_{\Delta}(k,k')=V(k,k')[1+2P_R(k,k')] + C(k,k'), \quad (8)$$

where $P_R(k,k')$ is the real part of the vertex function $P(k,k')$ defined in Eq. (4) and

$$C(k,k')=\sum_{k''} V(k,k'')V(k'',k')G(k'')G(k''-k-k') \quad (9)$$

is the so-called cross correction, which is a real function of k and k' . Finally, remembering that $G(k')G(-k')=|G(k')|^2$, we can see that the kernel of the linearized gap equation in Eq. (6) is also real and without loss of generality we can choose $\phi(k)$ as a real function of k .

In this article, we study both NCA and VCA as a function of band filling for a model density of states (DOS) which is constant through the entire electron bandwidth D . When the chemical potential ϵ_0 is close to the top (bottom) of the band, this model effectively mimics a hole (electron) doped two-dimensional parabolic band, provided ω_{ph} is smaller than the entire bandwidth. This modelization is thus a good starting point to eventually discuss filling effects in MgB_2 . Within the NCA framework, Marsiglio has already considered this model in his study of the superconducting instability.²⁰ What he found was that the critical temperature T_c decreases as the chemical potential ϵ_0 approaches the bottom or the top of the band. Naively, this reduction is expected since, close to the band edges, the average of the DOS over an energy window of order ω_{ph} gets reduced. Quantitatively, however, the reduction of T_c is also affected by nonrigid band effects induced by the electron-phonon coupling.

Within the theory of nonadiabatic superconductivity, this situation is drastically modified by the nontrivial band-filling dependence of the nonadiabatic corrections. To illustrate this point, let us consider the vertex function $P(k,k')$ defined in Eq. (4). In previous studies we have shown that, at half filling, the vertex correction has a marked dependence on the momentum transfer $\mathbf{q}=\mathbf{k}-\mathbf{k}'$, which is positive for $v_F|\mathbf{q}| < \omega_{\text{ph}}$ and negative for $v_F|\mathbf{q}| > \omega_{\text{ph}}$, where v_F is the Fermi velocity.¹⁶⁻¹⁸ If there is no preference to forward scatterings, the average over $|\mathbf{q}|$ of the vertex function is generally small and negative, reducing therefore the electron-phonon pairing and consequently T_c as compared to NCA.^{21,22} As the chemical potential is moved towards the top or bottom of the band, the \mathbf{q} dependence is more and more weakened and, when the distance between the band edge and ϵ_0 is sufficiently small, the vertex function assumes an overall positive sign with negligible momentum dependence.²³ In this regime therefore the nonadiabatic corrections tend to enhance the pairing, and

the reduction of T_c given by NCA is counter balanced by the nonadiabatic corrections. Close to the top or bottom of the band, we therefore expect a competition between band edge effects which depress T_c and nonadiabatic corrections which enhance T_c . Which of these two mechanisms prevails over the other depends on the chemical potential, on the bandwidth and on the electron-phonon interaction strength. It is matter of this article to provide quantitative results of this interesting problem.

Local approximation. To focus on the role of band filling in enhancing or decreasing T_c , we employ some approximations both in the description of the electron-phonon interaction and in the way of dealing with the normal and off-diagonal self-energies. First, we assume that phonon dynamics is well described by a single Einstein frequency ω_0 , so that the phonon propagator is

$$D(q)\equiv D(l)=-\frac{\omega_0^2}{\omega_l^2+\omega_0^2}, \quad (10)$$

where $\omega_l=2l\pi T$. In addition, we consider the electron-phonon matrix element as independent of the momenta, i.e., $g(\mathbf{k},\mathbf{k}')\equiv g$. This latter assumption disregards situations in which the electron-phonon interaction is strongly momentum dependent such as in strongly correlated metals in which large momentum transfers are suppressed by the rigidity of the correlated electronic wave function.^{14,24,25} Previous studies have shown that in this situation the surviving small momentum scattering has deep influences on the nonadiabatic corrections.¹⁶ In order to focus on the role of the band-filling effects, however, we assume in the following the electron-phonon matrix elements and the electronic Green's function to be independent of the electronic momenta. This assumption, which corresponds to the local approximation whose validity and limitations will be discussed later, permits the comparison with an exact solution in the limit of zero density. We note, however, that electronic models interacting with purely local interactions are widely studied as basis for the recent developed dynamical mean-field theory which provides in some cases an exact solution in infinite dimensions.²⁶⁻²⁸ The local approximation can be viewed as an average out of the momentum dependence over the whole Brillouin zone of electron-phonon matrix elements and of the electronic propagators. Thus we formally replace the electron propagators $G(k)$ by their local expressions $G_{\text{loc}}(n)=\sum_{\mathbf{k}}G(\mathbf{k},n)$ which depend only upon the Matsubara frequencies ω_n . The electron self-energy also becomes momentum independent and can be rewritten as

$$\Sigma(k)\rightarrow\Sigma(n)=i\omega_n-iW(n)+\chi(n), \quad (11)$$

where $W(-n)=-W(n)$ and $\chi(-n)=\chi(n)$. With this notation, G_{loc} reduces to

$$G_{\text{loc}}(n)=\int d\epsilon\frac{N(\epsilon)}{iW(n)-\epsilon+\epsilon_0-\chi(n)}, \quad (12)$$

where $N(\epsilon)$ is the bare electronic DOS and the integral over the energies ϵ is performed over the whole bandwidth D . We consider here a constant bare DOS system $N(\epsilon)=1/D$

$[-D/2 \leq \epsilon \leq D/2]$. The value of the chemical potential $\epsilon_0 = 0$ corresponds thus to a half-filling case whereas, for zero electron-phonon couplings $\epsilon_0 = -D/2$ and $\epsilon_0 = D/2$ represent, respectively, a completely empty and a completely filled band. When $|\epsilon_0 - D/2| \ll D$, this approximation simulates a quasi-two-dimensional parabolic band. By employing these assumptions, Eq. (12) reduces to

$$G_{\text{loc}}(n) = \frac{1}{D} \int_{-D/2}^{D/2} d\epsilon \frac{1}{iW(n) - \epsilon + \epsilon_0 - \chi(n)} \\ = -\frac{1}{D} [if(n) + g(n)], \quad (13)$$

where we have defined

$$f(n) = \arctan\left(\frac{D/2 - \epsilon_0 + \chi(n)}{W(n)}\right) + \arctan\left(\frac{D/2 + \epsilon_0 - \chi(n)}{W(n)}\right), \quad (14)$$

$$g(n) = \frac{1}{2} \ln \left[\frac{W(n)^2 + [D/2 - \epsilon_0 + \chi(n)]^2}{W(n)^2 + [D/2 + \epsilon_0 - \chi(n)]^2} \right]. \quad (15)$$

By substituting Eq. (13) into the definition of V_N of Eq. (3), the resulting interaction now depends only on Matsubara frequencies and reduces to

$$V_N(k, k') \rightarrow V_N(n, m) = g^2 D(n-m) [1 + \lambda P(n, m)], \quad (16)$$

where $\lambda = g^2 N(0) = g^2/D$ is the electron-phonon coupling constant and $P(n, m)$ is the vertex function

$$P(n, m) = -DT \sum_l D(n-l) G_{\text{loc}}(l) G_{\text{loc}}(l-n+m) \\ = P_R(n, m) + iP_I(n, m), \quad (17)$$

where

$$P_R(n, m) = -\frac{T}{D} \sum_l D(n-l) [g(l)g(l-n+m) \\ - f(l)f(l-n+m)] \quad (18)$$

and

$$P_I(n, m) = -\frac{T}{D} \sum_l D(n-l) [f(l)g(l-n+m) \\ + f(l-n+m)g(l)] \quad (19)$$

are the real and imaginary parts of the vertex function. Note that, since $g(-n) = g(n)$ and $f(-n) = -f(n)$, Eqs. (18),(19) imply $P_R(-n, -m) = P_R(n, m)$ and $P_I(-n, -m) = -P_I(n, m)$. Now, by applying the local approximation to Eqs. (2) and (11) we can write in a closed form the integral equations for $W(n)$ and $\chi(n)$:

$$W(n) = \omega_n - \lambda T \sum_m D(n-m) \{ [1 + \lambda P_R(n, m)] f(m) \\ + \lambda P_I(n, m) g(m) \}, \quad (20)$$

$$\chi(n) = \lambda T \sum_m D(n-m) \{ [1 + \lambda P_R(n, m)] g(m) \\ - \lambda P_I(n, m) f(m) \}. \quad (21)$$

The above equations are completed by the relation connecting the electron occupation number n with the chemical potential ϵ_0 :

$$n = 1 - \frac{2T}{D} \sum_n g(n), \quad (22)$$

where the factor 2 stems from the spin degeneracy. It is important to notice that from Eq. (22), half filling ($n=1$) is achieved by $g(n)=0$, which implies that the imaginary part of the vertex function P_I , Eq. (19), is zero. This is consistent with $\chi(n)=0$ and $\epsilon_0=0$ [see Eqs. (15),(21)].

Finally we consider the local approximation in the superconductive instability equations (6),(7). By following the previous steps, and by using Eqs. (13)–(15), it is straightforward to deduce that the gap equation becomes momentum independent and that it reduces to

$$\phi(n) = -T \sum_m V_\Delta(n, m) f(m) \frac{\phi(m)}{W(m)}, \quad (23)$$

where the pairing interaction in the local approximation reads

$$V_\Delta(n, m) = \lambda [1 + 2\lambda P_R(n, m)] D(n-m) + \lambda^2 C(n, m). \quad (24)$$

In the above expression, P_R is the real part of the vertex function given in Eq. (18), while $C(n, m)$ is the nonadiabatic cross correction resulting from the local approximation of the last term of Eq. (7):

$$C(n, m) = -TD \sum_l D(n-l) D(l-m) G_{\text{loc}}(l) G_{\text{loc}}(l-n-m) \\ = -\frac{T}{D} \sum_l D(n-l) D(l-m) [g(l)g(l-n-m) \\ - f(l)f(l-n-m)]. \quad (25)$$

When Eqs. (14), (15), (18), (19), (25) are plugged into Eqs. (20)–(23), we obtain a closed set of equations which can be numerically solved for both NCA and VCA to obtain the normal state self-energy and the superconducting transition. The numerical solution is achieved by using the usual procedures: first the normal state quantities $W(n)$, $\chi(n)$ are obtained by iteration by constraining the electron density n to have a given value. In a second step the gap equation (23) is rewritten as an eigenvalue equation and T_c is obtained when the highest eigenvalue becomes equal to unity.

Let us stress that this theory could provide a route to analyze the data from experiments via a theory which is valid even in a very low filling regime, where the Eliashberg and Mc Millan formulas for T_c are no longer valid. In fact given an electron-phonon coupling $g(\mathbf{k}, \mathbf{k}')$, as well as a calculated phonon spectrum, it is possible to evaluate an effective local interaction V_Δ by averaging over the *entire* Brillouin zone the product $V(k, k') = g(\mathbf{k}, \mathbf{k}')^2 D(k - k')$, where $D(k - k')$ is the corresponding phonon propagator. Notice that in this way filling effects will enter *both* in filling dependence of el-ph coupling and of the renormalized phonon frequencies. In this paper we conversely focus on the explicit band-filling dependence of the Fermi energy which are the driving effects at low density. To this aim we therefore choose a simple Lorentzian form for $V(k, k')$.

III. NORMAL STATE PROPERTIES

Our main aim is to investigate how the electron-phonon properties (effective mass, superconducting pairing, etc.) depend, in both NCA and VCA, on varying the chemical potential as a function of the electronic filling in comparison to the phonon energy scale ω_0 and to the large electron energy scale provided by the total bandwidth D . In this section we focus on normal state properties while the superconducting pairing will be discussed in Sec. IV. In relation to both these quantities we shall distinguish two regimes. One is at low electron filling n , where vertex diagrams enhance the effective electron-phonon coupling associated with the renormalization of the electron mass and the particle-particle superconducting pairing. The other is at large n , where the renormalization due to the vertex processes leads to an effective reduction of the coupling. We shall see that, while the magnitude of these electron-phonon effects depends on the strength of λ and on the size of the adiabatic parameter ω_0/D , the typical filling where the crossover between these two regimes occurs is only weakly dependent on the electron-phonon properties, suggesting that it is mainly determined by purely electronic methods. The relation of these results with the sign and magnitude of the vertex function will be discussed.

Concerning the normal state we present results for two physical quantities: the electron density as a function of the chemical potential and the effective mass ratio. The first quantity is obtained through Eq. (22) while the effective mass ratio is evaluated as the low-energy limit of the renormalized electronic frequencies [Eq. (20)]:

$$\frac{m^*}{m} = \frac{W(n)}{\omega_n} \Big|_{n=0}. \quad (26)$$

This expression provides a good estimation of the band mass as far as the sufficiently low temperature is concerned. We have iteratively solved Eqs. (20),(21) at several temperatures until we approached the asymptotic low temperature mass ratio. In this case we found that the electron density also converged to its low temperature limit. Calculations have been carried out at several values of the chemical potential for very low ($\omega_0/D=0.01$) and moderately large (ω_0/D

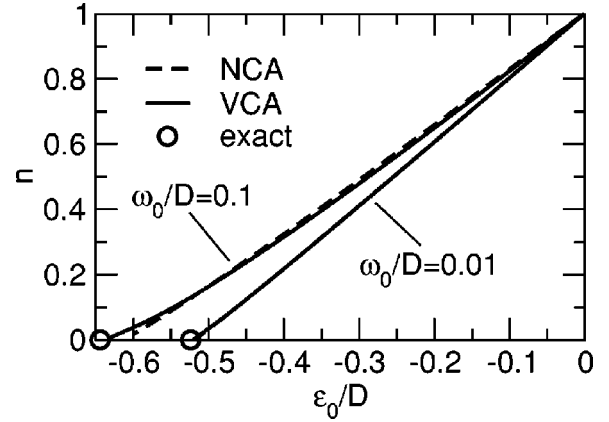


FIG. 1. Electron density as a function of the chemical potential ϵ_0 evaluated according to NCA and VCA for finite ($\omega_0/D=0.1$) and almost zero ($\omega_0/D=0.01$) adiabatic parameters. Empty circles represent the exact result of the zero density limit evaluated by means of the continued fraction within the local theory. The electron-phonon coupling is set at $\lambda = 1$.

$=0.1$) values of the phonon frequency and for two values of the coupling constant representative of weak ($\lambda=0.5$) and strong ($\lambda=1.0$) coupling.

In Fig. 1 we report on the behavior of the electron density as a function of the chemical potential evaluated using both NCA and VCA. No significant difference between the two approximations is observed. Note that for small values of n , ϵ_0 falls below the lower edge $\epsilon_0 = -D/2$ of the bare conduction band. This is especially evident when $\omega_0/D=0.1$ for which $\epsilon_0 < -D/2$ already for $n < 0.15$. In the zero density limit the chemical potential approaches the bottom band edge which corresponds to the ground state energy for a single electron in interaction with phonons. This energy is lowered with respect to the bare value ($\epsilon_0/D = -0.5$) by the electron-phonon interaction. Note that in the $n=0$ limit of this local theory the electron and phonon properties can be evaluated in a controlled way as well as in NCA and VCA by using the continued fraction technique (NCA and VCA correspond to different specific approximations of the continued fraction).²⁷ This is quite similar to the $d = \infty$ case, where the local ansatz is enforced by the infinite dimension limit.²⁶ The zero density exact result of the continued fraction is also reported in the figure (circles). Note that, at least for these value of ω_0/D and λ the vertex corrected theory already provides a rather good estimate of the exact results at zero density.²⁹ We can thus expect a polaron crossover around some critical value of the electron-phonon coupling λ_c which depends on the DOS shape. This feature, however, cannot be reproduced in NCA and VCA since it implies resummation of higher (infinite) order vertex diagrams.²⁷ The reliability of our approach is thus limited to the metallic regime of the electron-phonon system considered here. The value $\lambda_c \approx 1.544$, corresponding to the polaron transition in the adiabatic one particle electron-phonon system with rectangular DOS, represents thus an evaluation of upper limit of validity of our analysis near the adiabatic limit. Note, however, that for $\lambda < \lambda_c$ there is no reduction of the zero density ground state energy due to the electron-phonon interaction in

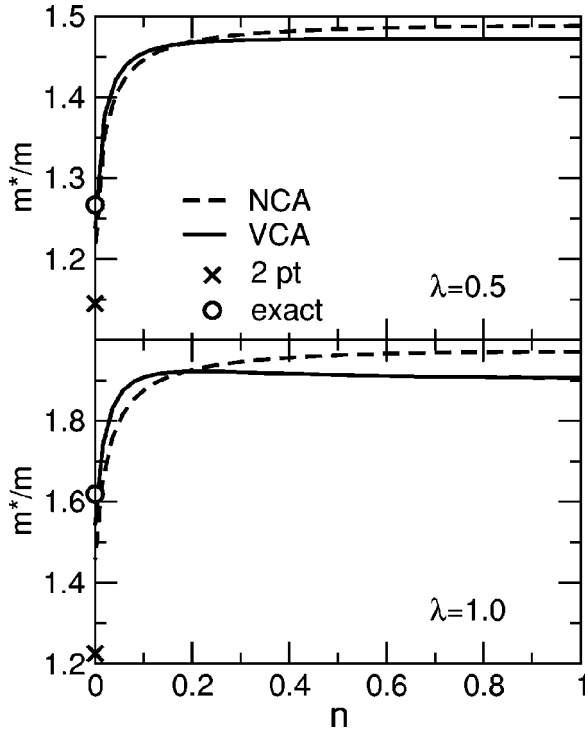


FIG. 2. Effective mass ratio for $\omega_0/D=0.01$ according the non-crossing and vertex corrected approximations. In the zero electron density limit data are also shown for exact calculations by means of continued fraction and for the second order perturbation theory (2PT).

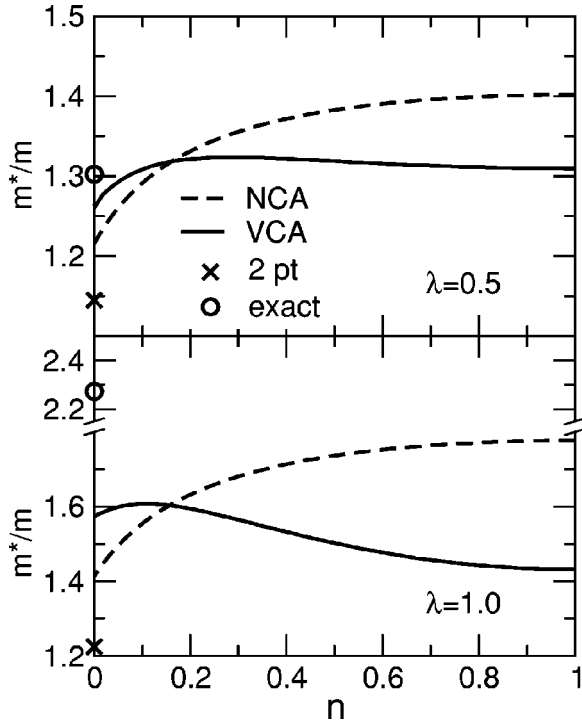


FIG. 3. Effective mass ratio for $\omega_0/D=0.1$. Notations are the same as in Fig. 2.

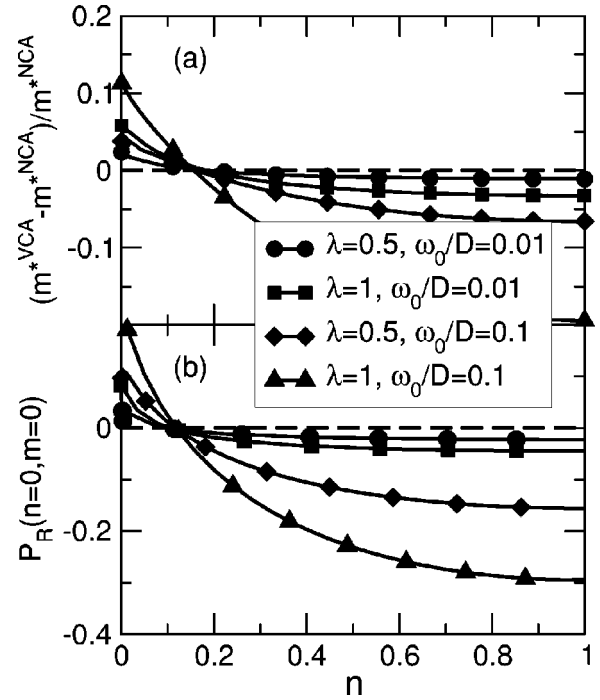


FIG. 4. (a) Relative difference between effective electron masses evaluated according to VCA and NCA as a function of the electron filling. (b) Sign of the real part of the vertex function $P_R(n, m)$ [Eq. (18)] evaluated at zero frequencies $n=0, m=0$.

the strictly adiabatic limit, i.e., when $\omega_0/D \rightarrow 0$.³⁰ This result, which includes all order vertex corrections, holds true even when the local approximation is relaxed. Therefore we expect that the frozen phonon approximation cannot reproduce this low density behavior at least for couplings outside the polaronic regime.

After having discussed the n - ϵ_0 phase diagram and the range of validity of our analysis, we now address the filling dependence of the effective mass ratio m^*/m . In Figs. 2 and 3 the results of the calculations for $\omega_0/D=0.01$ and $\omega_0/D=0.1$, respectively, are reported. Because of band edge effects the effective electron mass m^* is reduced in NCA as the filling approaches $n \rightarrow 0$. Increasing the phonon frequency leads to a broadening of this trend. The introduction of vertex diagrams can affect this scenario. In particular, as shown in Fig. 3 (lower panel), for large enough electron-phonon coupling and adiabatic parameter ω_0/D the effective electron mass m^* in VCA can be *larger* at the band bottom than at half filling suggesting that the increase of the effective electron-phonon coupling in this regime is because of the vertex diagrams.

The comparison between NCA and VCA can provide an estimate of the vertex effects alone. In particular for both low and intermediate phonon frequencies we can distinguish a low doping regime in which the inclusion of the vertex diagrams increases the effective mass²⁹ and a high doping regime in which the effective mass is reduced by the inclusion of the vertex corrections.³³

In order to single out the effects of the nonadiabatic diagrams as a function of the electron filling, we plot the relative differences for VCA and NCA results concerning the

renormalization of the electronic mass $m^*[(m^{*\text{VCA}} - m^{*\text{NCA}})/m^{*\text{NCA}}]$ in Fig. 4(a). This plot clearly shows the two regimes previously mentioned: a low electron density regime where the introduction of nonadiabatic vertex diagrams (VCA) leads to an enhancement of the electron-phonon coupling with respect to NCA for single particle properties (m^*/m) and a large electron density regime where the opposite holds true. An interesting result is that the crossover filling $n_c \sim 0.15-0.2$ where nonadiabatic vertex effects change from positive $[(m^{*\text{VCA}} - m^{*\text{NCA}})/m^{*\text{NCA}} > 0]$ to negative $[(m^{*\text{VCA}} - m^{*\text{NCA}})/m^{*\text{NCA}} < 0]$ is almost independent of the bare electron-phonon coupling λ and of the adiabatic ratio ω_0/D . We would like to stress again that for these values of n the chemical potential ϵ_0 , in particular for $\omega_0 = 0.01D$, can be quite far from the bottom of the band with respect to the phonon energy, so that the crossover is not simply related to band edge effects as described by a rigid band picture.

In order to better clarify the origin of this crossover from a VCA m^* -enhancement region ($n \leq 0.15-0.2$) to a VCA m^* -reduction one ($n \geq 0.15-0.2$), we plot the size of the vertex function $P_R(n, m)$ [Eq. (18)] evaluated in the static limit $n=0, m=0$ in Fig. 4(b). Previous studies showed that the static limit can indeed be representative of the effects of the vertex function on static quantities such as m^* . The comparison of panels (a) and (b) of Fig. 4 points out striking similarities between the filling behavior of the two quantities. It is thus easy to identify the sign of P_R as the direct origin of the enhancement or suppression of the VCA electronic mass m^* with respect to NCA. Once more we would like to stress that while the magnitude of the discrepancy between NCA and VCA [panel (a)] or P_R [panel (b)] depend on the adiabatic parameter ω_0/D and on the electron-phonon strength λ , the electron filling $n_c \sim 0.15-0.2$ where vertex diagrams are almost perfectly balanced is only weakly dependent on electron-phonon properties.

Another interesting issue to be investigated is the dependence of the electron-phonon renormalization on the degree of the diagrammatic approximations employed. Such a dependence can be traced out in a controlled way in the zero electron density limit where different theories correspond to different degrees of diagrammatic approximations.^{27,29} We thus compare the NCA and VCA with (i) second order perturbation theory (2PT), where only the lowest order diagram with bare propagators is taken into account, namely, in Eqs. (20), (21) the right-hand side is evaluated with $W_n = \omega_n$, $\chi = 0$, and $P_R = P_I = 0$ and (ii) with the exact result for the local theory obtained by the infinite resummation of the continued fraction.

For all the adiabatic parameters ω_0/D and coupling λ considered here (Figs. 2,3) we observe a monotonous increase of the effective mass enhancement m^*/m from second order perturbation theory, to NCA, VCA, ending up with the exact result. This suggests that vertex diagrams in the zero density limit are defined to be positive (the well defined positive sign of the vertex function in the zero density limit was analytically pointed out in Ref. 34) and the resummation of higher and higher vertex diagrams, as taken into account by

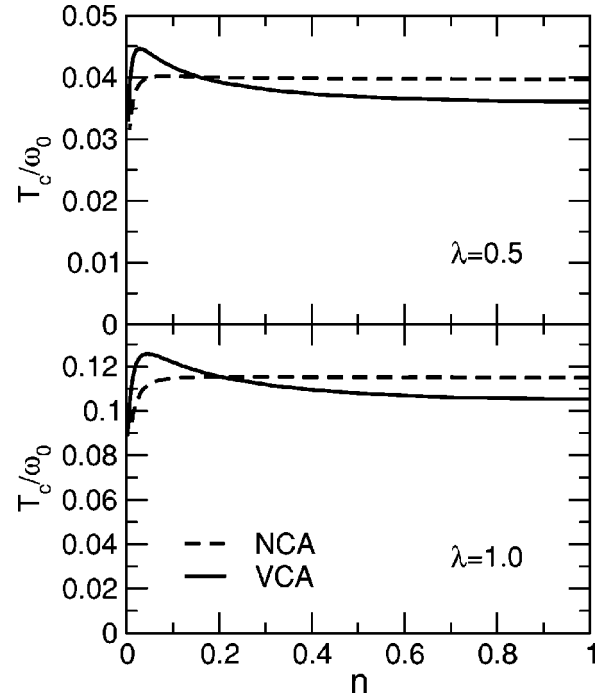


FIG. 5. Critical temperature T_c/ω_0 vs the electron filling n for $\omega_0/D=0.01$ in NCA and VCA.

the continued fraction, converges uniformly for the values of λ and ω_0/D considered here. In this situation the vertex corrected theory can be considered qualitatively representative of the infinite resummation exact result.²⁹ This picture is expected to be less and less accurate as soon as one approaches the polaronic regime. For instance, we note that in the almost adiabatic case ($\omega_0/D=0.01$) VCA already pro-

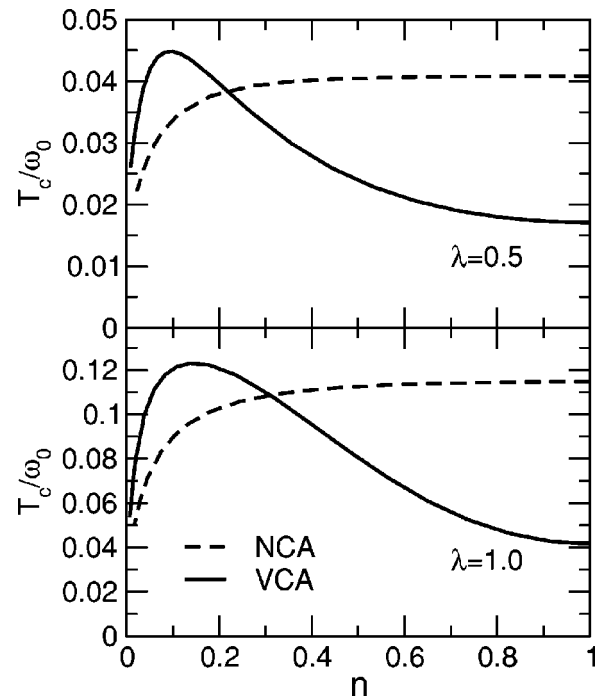


FIG. 6. Same as Fig. 5 for $\omega_0/D=0.1$.

vides a good estimation of the zero density exact result even for large coupling $\lambda=1.0$. This can be understood by remembering that electron-phonon polaron correlations are frozen in the adiabatic limit up to $\lambda \leq \lambda_c$, while they diverge at $\lambda = \lambda_c$.^{27,30} On the contrary, for $\omega_0/D=0.1$ the approaching of the polaron crossover is reflected in different properties (here, for instance, in the electron mass renormalization) even for $\lambda < \lambda_c$. This means that the qualitative trend from 2PT to NCA, VCA, and to the exact result at $n=0$ is still preserved, but it lacks under the quantitative side as far as λ getting closer to λ_c .²⁹

Summarizing the results of this section, we have identified two distinct regions of the electronic filling where the vertex diagrams are, respectively, positive and negative, leading to a corresponding increase or reduction of m^* with respect to NCA. We have also shown that the extension of this filling region does not vanish in the adiabatic limit. The positivity of the vertex diagrams can be better understood in the zero density limit. This is a quite general result and we believe that the physics of this limit can be qualitatively representative of the low doping region ($n \leq 0.15-0.2$) at least in the case where no phonon renormalization effects are explicitly taken into account (note, however, that the phonon screening vanishes as the charge density goes to zero). Once again we stress that at large filling $n \geq 0.15-0.2$ the system behaves in quite a different way, since, for instance, the inclusion of vertex diagrams leads to a *reduction* of the effective mass m^* instead of an enhancement of it.

IV. CRITICAL TEMPERATURE

The competition between band edge effects and nonadiabatic contributions on the critical temperature shares striking similarities with the case of the effective electron mass m^* . In Figs. 5 and 6 we report the results for T_c in both NCA and VCA frameworks, respectively for $\omega_0/D=0.01$ and for $\omega_0/D=0.1$, as a function of the electron density n .

In analogy with the renormalized electron mass m^*/m , the NCA results show that T_c reduces as the electron occupation number n deviates from half filling ($n=1$). This can again be naively understood in terms of reduced density of states as the band edge is approached within a phonon energy window. The resemblance with the n dependence of m^*/m is also maintained when nonadiabatic corrections are included: at half filling T_c is reduced with respect to NCA while, at sufficiently low n , T_c is enhanced. This result is in agreement with previous studies on the density effects on nonadiabatic corrections.^{21,23} At first sight it could appear surprising that an enhancement of the critical temperature is found in the presence of a corresponding enhancement of the effective mass m^* since strong renormalization of m^* is usually associated with a depletion of spectral weight. However, it was shown that even in adiabatic theory in the strong coupling limit both critical temperature ($T_c \propto \sqrt{\lambda}$) and effective mass ($m^*/m \propto \lambda$) increase.³¹ In addition it was pointed out in Ref. 32 and later explicitly shown in Refs. 16–18 that a different mechanism based on nonadiabatic contributions leads to a reduction of the spectral weight which is counterbalanced by the additional opening of nonadiabatic interaction channels

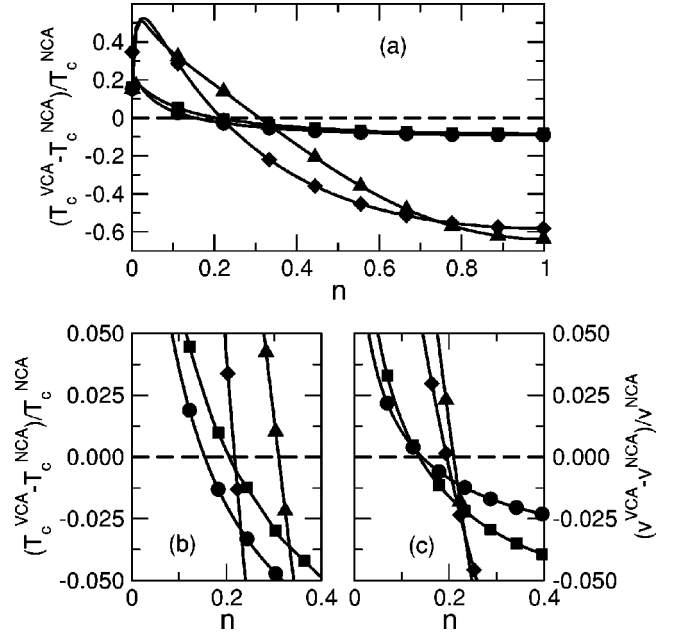


FIG. 7. (a) Relative difference between T_c evaluated in VCA and NCA $(T_c^{VCA} - T_c^{NCA})/T_c^{NCA}$. (b) Relative difference between the maximum eigenvector v_{\max} of Eq. (24) evaluated in VCA and NCA $(v_{\max}^{VCA} - v_{\max}^{NCA})/v_{\max}^{NCA}$. The symbols are as in Fig. 4.

in the Cooper pairing even at intermediate coupling.

Although m^*/m and T_c behave in a qualitative similar manner, interesting differences can be singled out by looking at the relative change of T_c due to the vertex diagram inclusion $(T_c^{VCA} - T_c^{NCA})/T_c^{NCA}$ [Fig. 7(a)]. We observe that the filling n_c at which the inclusion of vertex diagrams changes its character from positive to negative with respect to the superconducting critical temperature is now quite sensitive of the electron-phonon coupling λ and of the adiabatic ratio ω_0/D . In particular, n_c increases as λ and ω_0/D increase. This is in contrast with the case of the electron mass where n_c was almost independent of electron-phonon quantities. There are two basilar reasons which account for this difference. First, we remind the reader that, while the electron mass renormalization is a *static* quantity (e.g., it is evaluated at zero frequency), the calculation of T_c involves the knowledge of the electron-phonon kernel (and of the vertex function) in an energy window $\sim \pm \omega_0$. The overall structure of the vertex function can thus be remarkably dependent on λ and ω_0/D affecting the global balance for which $T_c^{VCA} = T_c^{NCA}$. An additional source of discrepancy comes from the fact that T_c is by definition a finite temperature quantity. The value of T_c itself is thus a λ - ω_0/D dependent quantity and finite temperature effects can be drastically important in Fig. 7(a).

In order to single out these finite temperature effects we evaluate the maximum eigenvalue v_{\max} of the superconducting electron-phonon kernel $V_{\Delta}(n, m)$ [Eq. (24)] at low temperature in the normal state. This provides an estimate of the superconducting pairing which is not affected by finite temperature effects. A zoom of the interesting region $[(v_{\max}^{VCA} - v_{\max}^{NCA})/v_{\max}^{NCA} \sim 0]$ is shown in Fig. 7(c) as well as a corre-

sponding zoom of $(T_c^{\text{VCA}} - T_c^{\text{NCA}})/T_c^{\text{NCA}} \sim 0$. As a first remark we note that, contrary to Fig. 7(b), in Fig. 7(c) there is only a weak dependence of n_c on the electron-phonon coupling λ . As a matter of fact the dependence on λ in Fig. 7(b) mainly stems from finite temperature effects, with a large $\lambda = 1.0$ associated with higher temperatures ($T_c \approx 0.1-0.12$) in comparison with $T_c \approx 0.03-0.04$ for small $\lambda = 0.5$. Once finite temperature effects are disregarded, we still note a significant dependence on the adiabatic ratio ω_0/D in Fig. 7(c) which does not appear, for instance in Fig. 4. As above discussed, we trace this residual dependence on ω_0/D back to the important role of the frequency dependence in the superconducting kernel. Interesting, in the almost adiabatic regime $\omega_0/D = 0.01$, the same value of $n_c \approx 0.15$ as found for the electronic mass and for $P_R(n=0, m=0)$ is recovered, signaling the static nature of that value. It is significant that by taking into account both the retarded nature of the superconducting pairing and finite temperature effects yields an increase of the low doping region where the nonadiabatic vertex diagram enhance the electron-phonon coupling. The value $n \lesssim 0.15-0.2$ can thus be considered as a conservative estimate of this regime.

In order to focus on the effects of nonadiabatic electron-phonon contributions, we have not considered the role of Coulomb repulsion between electrons in this work. In the simplest scheme, the electron-electron repulsion can be included by adding an Hubbard U term in Eq. (6), as done in Ref. 20. By treating U as a parameter independent of electron filling we have performed calculations of T_c in both NCA and VCA. We have found that the inclusion of U leads to an overall reduction of T_c and to a magnification of the differences between NCA and VCA reported in this section. However, no qualitatively new physics is induced by U , although we expect an additional reduction of T_c when the electron density is sufficiently low to poorly screen the Coulomb interaction. However, the role of screening was not the aim of this paper, and its effects will be investigated in a future publication.

V. DISCUSSION AND CONCLUSIONS

In this paper we have addressed the role of band filling in some normal and superconducting properties of electron-phonon systems. In particular, within a local approximation, we have identified two regions of the electron band filling in which electron-phonon properties behave in qualitatively different manners. At sufficiently low density, the inclusion of vertex diagrams beyond the noncrossing approximation leads to a strengthening of the electron-phonon effects reflected by an enhancement of the effective electron mass m^* and of the superconducting critical temperature T_c . On the contrary, close to half filling, the vertex corrected approximation results in a net decrease of m^* and T_c with respect to the noncrossing approximation. We have shown that these different behaviors are governed by the net sign of the vertex diagrams which is positive in the low density regime and negative close to half filling. The density value $n_c \approx 0.15-0.2$ separating these two regimes depends only weakly on the microscopic electron-phonon parameters

which, on the other hand, rule the size of the corresponding enhancement or decrease of m^* and T_c .

The results for the low electron density regime are compared with the zero density limit for which the exact solution of this local problem is known. In this limit we have shown that the inclusion of diagrams with higher and higher order, from second order perturbation theory to the noncrossing approximation and to the vertex corrected theory, monotonically approaches the exact results. Such an improvement as function of the degree of approximation suggests that the positive sign of the vertex function leads to a series with positive terms, which should steadily approach the exact solution if a resummation of infinite order diagrams were performed.²⁹

The enhancement of the effective electronic mass m^* and of the superconducting critical temperature T_c in the low electron density region is expected to be relevant in two-dimensional systems where small charge density is accompanied by a finite density of states at the bottom (or top) of the band. Thus, in principle, our results could concern the high- T_c compound MgB_2 and the hypothetical doped LiBC recently proposed to superconduct with even higher T_c .¹⁰ In particular in MgB_2 the hole carrier density related to the σ bands $n_h \approx 0.08 < n_c$ (Ref. 3) sets the system in a region where these effects are relevant, although the large bandwidth of the σ bands in MgB_2 compared with the relevant phonon frequency leads to $\omega_0/D \sim 0.01$, corresponding to a quite weak effect on m^* and T_c . These effects can, however, be further enhanced via Al substitution. Interestingly, the experimentally observed reduction of T_c as a function of Al doping^{7,8} cannot be accounted for within a McMillan scheme⁹ even when the Coulomb pseudopotential μ^* is introduced to account for $T_c \approx 39$ K in the undoped MgB_2 compound.

A quantitative enhancement of T_c from vertex corrections in MgB_2 could be argued by considering two distinct effects not considered in the present paper, namely, (a) the intrinsic momentum dependence of the *bare* electron-phonon matrix elements and (b) the momentum dependence of the renormalized electron-phonon vertex. Let us discuss them separately.

(a) Several first principle calculations have shown that the electron-phonon coupling in MgB_2 has a strong momentum dependence and is particularly strong near the Γ point at $\mathbf{q} = 0$.^{4,5} In this situation, neglecting the momentum dependence of the electron-phonon matrix elements $g_{\mathbf{k},\mathbf{k}'} \sim g$ becomes a poor ansatz just as in the case of strongly correlated electron systems.^{14,24,25} A proper inclusion of the predominance of forward scattering at small \mathbf{q} has been shown to lead to an intrinsic selection of the positive sign for the vertex diagrams and to favor a corresponding enhancement of m^* and T_c .¹⁶

(b) Even neglecting the momentum dependence of the *bare* electron-phonon matrix elements the renormalized vertex acquires a momentum dependency due to vertex corrections. The local approximation treat these effects by averaging the intrinsic dependence of the vertex diagrams on the momentum transfer $\mathbf{q} = \mathbf{k} - \mathbf{k}'$. In extreme cases the local assumption can estimate the total phase space available for

these vertex processes incorrectly and hence the magnitude of the vertex diagrams. This is the most evident, for instance, in the low density adiabatic regime where the available transferred momenta are limited, in the weak coupling regime, by $\sim |\mathbf{q}| \leq 2k_F$, while the local approximation would integrate them over the whole Brillouin zone. In this limit, for instance, it is easy to show that the local approximation provides an underestimate for the magnitude of the vertex diagrams.

Both effects could be separately considered to properly account for vertex corrections in MgB_2 . Work in this direction is in progress.

ACKNOWLEDGMENTS

This work was partially supported by Project Nos. COFIN-2001 MIUR and PRA-UMBRA INFM.

-
- ¹J. Nagamatsu, N. Nakagawa, T. Muranaka, Y. Zenitani, and J. Akimitsu, *Nature (London)* **410**, 63 (2001).
- ²K.D. Belashchenko, M. van Schilfgaarde, and V.P. Antropov, *Phys. Rev. B* **64**, 092503 (2001).
- ³J.M. An and W.E. Pickett, *Phys. Rev. Lett.* **86**, 4366 (2001).
- ⁴Y. Kong, O.V. Dolgov, O. Jepsen, and O.K. Andersen, *Phys. Rev. B* **64**, 020501 (2001).
- ⁵K.-P. Bohnen, R. Heid, and B. Renker, *Phys. Rev. Lett.* **86**, 5771 (2001).
- ⁶A.Y. Liu, I.I. Mazin, and J. Kortus, *Phys. Rev. Lett.* **87**, 087005 (2001).
- ⁷P. Postorino, A. Congeduti, P. Dore, A. Nucara, A. Bianconi, D. Di Castro, S. De Negri, and A. Saccone, *Phys. Rev. B* **65**, 020507(R) (2001).
- ⁸J.Q. Li, L. Li, F.M. Liu, C. Dong, J.Y. Xiang, and Z.X. Zhao, *Phys. Rev. B* **65**, 132505 (2002).
- ⁹G. Profeta, A. Continenza, and S. Massidda, *Phys. Rev. B* **68**, 144508 (2003).
- ¹⁰H. Rosner, A. Kitaigorodsky, and W.E. Pickett, *Phys. Rev. Lett.* **88**, 127001 (2002).
- ¹¹A.B. Migdal, *Zh. Éksp. Teor. Fiz.* **34**, 1438 (1958) [*Sov. Phys. JETP* **7**, 996 (1958)].
- ¹²I.G. Lang and Yu.A. Firsov, *Zh. Éksp. Teor. Fiz.* **43**, 1843 (1962) [*Sov. Phys. JETP* **16**, 1301 (1963)].
- ¹³O. Gunnarsson, *Rev. Mod. Phys.* **69**, 575 (1997).
- ¹⁴M.L. Kulić, *Phys. Rep.* **338**, 1 (2000).
- ¹⁵G.M. Zhao, M.B. Hunt, H. Keller, and K.A. Müller, *Nature (London)* **381**, 676 (1996); D. Louca, T. Egami, E.L. Brosha, H. Röder, and A.R. Bishop, *Phys. Rev. B* **56**, 8475 (1997); S.J.L. Billinge, R.G. DiFrancesco, G.H. Kwei, J.J. Neumeier, and J.D. Thompson, *Phys. Rev. Lett.* **77**, 715 (1996).
- ¹⁶C. Grimaldi, L. Pietronero, and S. Strässler, *Phys. Rev. Lett.* **75**, 1158 (1995).
- ¹⁷L. Pietronero, S. Strässler, and C. Grimaldi, *Phys. Rev. B* **52**, 10 516 (1995).
- ¹⁸C. Grimaldi, L. Pietronero, and S. Strässler, *Phys. Rev. B* **52**, 10 530 (1995).
- ¹⁹G.M. Eliashberg, *Zh. Éksp. Teor. Fiz.* **38**, 966 (1960) [*Sov. Phys. JETP* **11**, 696 (1960)].
- ²⁰F. Marsiglio, *J. Low Temp. Phys.* **87**, 659 (1992).
- ²¹J.K. Freericks, *Phys. Rev. B* **50**, 403 (1994).
- ²²P. Paci, E. Cappelluti, C. Grimaldi, and L. Pietronero, *Phys. Rev. B* **65**, 012512 (2001).
- ²³A. Perali, C. Grimaldi, and L. Pietronero, *Phys. Rev. B* **58**, 5736 (1998).
- ²⁴M. Grilli and C. Castellani, *Phys. Rev. B* **50**, 16 880 (1995).
- ²⁵R. Zeyher and M.L. Kulić, *Phys. Rev. B* **53**, 2850 (1996).
- ²⁶A. Georges, G. Kotliar, W. Krauth, and M.J. Rozenberg, *Rev. Mod. Phys.* **68**, 13 (1996).
- ²⁷S. Ciuchi, F. de Pasquale, S. Fratini, and D. Feinberg, *Phys. Rev. B* **56**, 4494 (1997).
- ²⁸Q. Si, G. Kotliar, and A. Georges, *Phys. Rev. B* **46**, 1261 (1992).
- ²⁹M. Capone, S. Ciuchi, and C. Grimaldi, *Europhys. Lett.* **42**, 523 (1998).
- ³⁰V.V. Kabanov and O.Yu. Mashtakov, *Phys. Rev. B* **47**, 6060 (1993).
- ³¹J.P. Carbotte, *Rev. Mod. Phys.* **62**, 1027 (1990).
- ³²L. Pietronero and S.S. Strässler, *Europhys. Lett.* **18**, 627 (1992).
- ³³C. Grimaldi, E. Cappelluti, and L. Pietronero, *Europhys. Lett.* **42**, 667 (1998).
- ³⁴C. Grimaldi, L. Pietronero, and M. Scattoni, *Eur. Phys. J. B* **10**, 247 (1999).